Mineralogy and Petrology (2022) 116:1–14
https://doi.org/10.1007/s00710-021-00766-8

ORIGINAL PAPER

The key role of μH_2O gradients in deciphering microstructures and mineral assemblages of mylonites: examples from the Calabria polymetamorphic terrane

Fabrizio Tursi[1]

Received: 4 June 2021 / Accepted: 3 October 2021 / Published online: 20 October 2021

Abstract
A careful petrologic analysis of mylonites' mineral assemblages is crucial for a thorough comprehension of the rheologic behaviour of ductile shear zones active during an orogenesis. In this view, understanding the way new minerals form in rocks sheared in a ductile manner and why relict porphyroblasts are preserved in zones where mineral reactions are generally supposed to be deformation-assisted, is essential. To this goal, the role of chemical potential gradients, particularly that of H_2O (μH_2O), was examined here through phase equilibrium modelling of syn-kinematic mineral assemblages developed in three distinct mylonites from the Calabria polymetamorphic terrane. Results revealed that gradients in chemical potentials have effects on the mineral assemblages of the studied mylonites, and that new syn-kinematic minerals formed in higher-μH_2O conditions than the surroundings. In each case study, the banded fabric of the mylonites is related to the fluid availability in the system, with the fluid that was internally generated by the breakdown of OH-bearing minerals. The gradients in μH_2O favoured the origin of bands enriched in hydrated minerals alternated with bands where anhydrous minerals were preserved even during exhumation. Thermodynamic modelling highlights that during the prograde stage of metamorphism, high-μH_2O was necessary to form new minerals while relict, anhydrous porphyroblasts remained stable in condition of low-μH_2O even during exhumation. Hence, the approach used in this contribution is an in-depth investigation of the fluid-present/-deficient conditions that affected mylonites during their activity, and provides a more robust interpretation of their microstructures, finally helping to explain the rheologic behaviour of ductile shear zones.

Keywords Chemical potentials · Mineral reactions · Ductile shear zones · Porphyroblasts · Calabria polymetamorphic terrane

Introduction

Ductile shear zones are the locus of the Earth's lithosphere where stress is largely accommodated, representing domains that tend to remain weaker than the host rocks even after their formation. This contribution is focussed on the petrologic nature of syn-kinematic minerals in mylonites, resulting from chemical processes related to strain weakening in already formed ductile shear zones, both under compressive- and extensional-dominating tectonics. The chemical processes in question are nothing more than mineral reactions. The interplay between deformation and mineral reactions was proposed from the merely development of foliations in metamorphic rocks (Etheridge et al. 1984; Bell and Cuff 1989; Bell and Hayward 1991), up to strain localisation in ductile shear zones (de Ronde et al. 2005; Holyoke and Tullis 2006a, b). In the latter case, the formation of fine-grained reaction products along the foliation plane in ductile shear zones either natural (Keller et al. 2004) or experimentally produced (Brodie and Rutter 1987; de Ronde et al. 2005; Holyoke and Tullis 2006a, b), can largely accommodate strain when the reaction products interconnect (de Ronde et al. 2005). According to Wheeler (2014) and Hobbs and Ord (2017), the way mineral reactions in highly strained rocks take place is by deformation-driven variations of chemical potentials at the solid interfaces. On the other hand, Powell et al. (2018) demonstrated the small

Editorial handling: S. W. Faryad

✉ Fabrizio Tursi
fabrizio.tursi@uniba.it

[1] Dipartimento Di Scienze Della Terra E Geoambientali, 70125 Bari, Italy

effect of non-lithostatic thermodynamics on mineral equilibria in metamorphic systems. Rubie (1998) also highlighted how nucleation kinetics is delayed in metamorphic rocks, even under high-strain ductile deformation and fluid influx, allowing the survival of metastable mineral assemblages. However, under fluid-present conditions, reaction kinetics is commonly enhanced (Rubie 1986; Guiraud et al. 2001), accompanied by complete variation of mineral assemblages when large fluid-rock interactions occur (e.g. Tursi et al. 2018, and references therein). Under fluid-deficient conditions, relict metastable minerals survive instead, in association with some new, syn-kinematic reaction products (e.g. Pennacchioni and Cesare 1997; Hentschel et al. 2020; Tursi et al. 2020a, b). This is the central issue concerned to this paper, a topic still debated amongst metamorphic petrologists (Powell et al. 2019), which here is explored in rocks naturally deformed through simple shear. In this regard, as deformation favours diffusion of elements along grain boundaries and permeability is enhanced during ductile shearing (Etheridge et al. 1983), chemical potential gradients can be either eliminated or favoured in the rock (Powell et al. 2019), producing equilibrium or disequilibrium mineral assemblages, respectively (Regenauer-Lieb et al. 2009; Hobbs and Ord 2017). Hence, chemical potential grids were calculated in the present research to detect the control of the chemical potential of some mobile major components, like major elements or H_2O, on the mineral assemblages of three mylonites from the polymetamorphic terrane of Calabria, that experienced shearing under overall fluid-deficient conditions either under compressive- or extensional-dominating tectonics.

Brief geological setting and examined case studies

The Calabria–Peloritani terrane is composed of three stacked tectonic complexes (Fig. 1a), namely, from the top to the bottom: (i) the Upper Complex, consisting of Variscan granulite to greenschist-facies metamorphic rocks and interleaved granitoids (e.g. Schenk 1980; Fornelli et al. 2020); (ii) the Intermediate Complex, primarily composed of Alpine ophiolite units (Liberi et al. 2006); and (iii) the Lower Complex, characterised by phyllites and unmetamorphosed to metamorphosed carbonate rocks underthrusted during Apennines building (Iannace et al. 2007). The three examined ductile shear zones developed in rocks with different bulk rock composition, ranging from mafic (T-MORB affinity, e.g. Fedele et al. 2018) to felsic (granitic, e.g. Tursi et al. 2021), and are represented by the Levadio Shear Zone, the La Guardiola Shear Zone and the Curinga–Girifalco Line. The Levadio Shear Zone developed during the Variscan orogeny (Festa et al. 2018; Tursi et al. 2020b) while, the La Guardiola Shear Zone and the Curinga–Girifalco Line developed during the Alpine orogeny (Festa et al. 2020; Tursi et al. 2020a). The research studies of Tursi and co-authors on these diverse ductile shear zones, which are some amongst those exposed in Calabria (e.g. Prosser et al. 2003; Liotta et al. 2004; Festa et al. 2006; Ortolano et al. 2020), have highlighted the common development of OH-bearing minerals during each shearing event, although characterised by overall fluid-deficient conditions. The results of these studies, along with the petrographic features of the investigated mylonites, are briefly summarised below, following an increasing metamorphic grade.

The La Guardiola Shear Zone

In Catena Costiera (Fig. 1b), at La Guardiola Cliff, the Diamante–Terranova Unit blueschists are tectonically juxtaposed to marbles and calcschists of the Lower Complex, with the blueschists characterised by a well-defined mylonitic foliation (Fig. 2a). Sample DIA1a (Tables 1, 2) from Tursi et al. (2020a) is considered here as representative of the mylonitic blueschists cropping out at La Guardiola Cliff (Fig. 2a). The mineral assemblage of this rock consists of gl + law + chl + pmp + q + sph ± ab ± ep (Fig. 2b–d) with fine-grained recrystallised glaucophane-rich bands alternating with pumpellyite-rich ones where large, up to one-millimetre sized, pre-kinematic lawsonite porphyroblasts occur (Fig. 2b–d). The rock is characterised by a banded fabric, and by albite-rich veins that crosscut the glaucophane-rich bands and connect the pumpellyite-rich ones (Fig. 2a–c). The mylonitic stage developed from ~ 1.1 GPa and ~ 380 °C, the last stages of exhumation recorded in the coarse-grained lawsonite–clinopyroxene blueschist lenses, up until ~ 0.6–0.7 GPa and 290–315 °C, where the albite-rich veins are inferred to have formed in the banded mylonitic blueschists (Fig. 2e, Tursi et al. 2020a), with the overall banded texture of the latter accounting for disequilibrium. Three dehydration equilibria, highlighted by Tursi et al. (2020a), broke down lawsonite and glaucophane in the glaucophane-rich bands, and released large quantities of H_2O in the system; they were responsible for the formation of chlorite, pumpellyite and quartz within the pumpellyite-rich bands. Therefore, the authors interpreted the pumpellyite-rich bands of the sheared blueschists as the storage loci of the fluid released by the glaucophane-breakdown reactions within the high-strain ultramylonitic bands during fast exhumation (Fig. 2). The microstructure related to the set of albite-rich veins connecting the pumpellyite-rich bands and transecting the glaucophane-rich ones (Fig. 2a–c), was interpreted as due to the evolution in the rheologic behaviour of the glaucophane-rich bands during exhumation from fluid-present to fluid-deficient conditions. On the other hand,

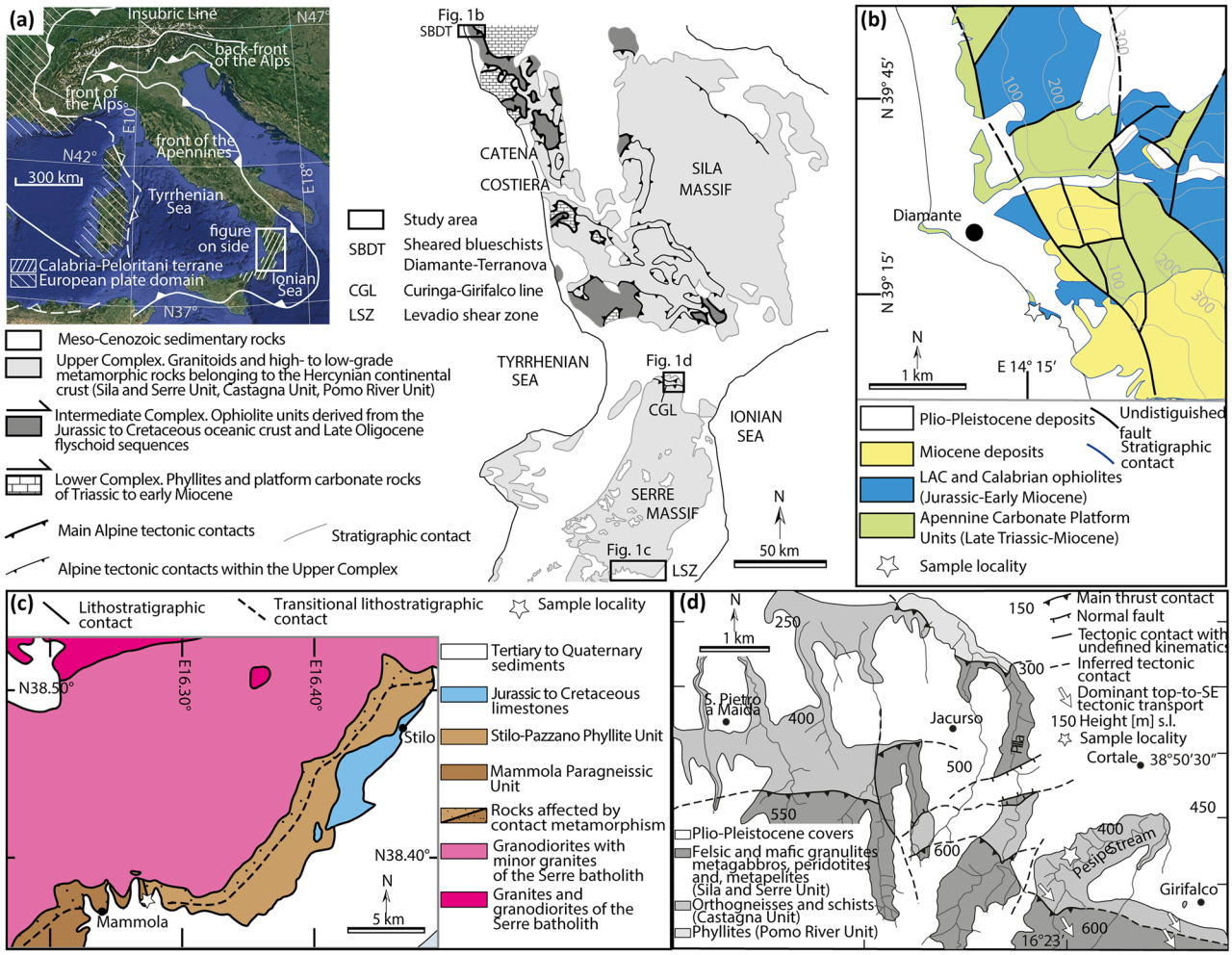

Fig. 1 (**a**) Sketch of the current position of the Apennines and Alpine fronts, according to Carminati and Doglioni (2012); on the right side, the geological sketch map of central and northern Calabria-Peloritani terrane, modified after Festa et al. (2004), is shown along with the study areas of ductile shear zones. (**b**) Primary geological units outcropping in the Diamante area (modified after Fedele et al. 2018 and Tursi et al. 2020a); the location of the sampled area is also indicated (according to Tursi et al. 2020a). (**c**) Geological sketch map of the southern Serre Massif (modified after Graessner and Schenk 1999 and Langone et al. 2014); the mapped area is highlighted (after Festa et al. 2018). (**d**) Structural sketch map of the CGL nearby Girifalco village, modified after Festa et al. (2020)

fluid-present conditions were supposed by the authors to be restricted to the pumpellyite-rich bands during shearing.

The Levadio Shear Zone

In the southern Serre Massif (Fig. 1c), during Late Variscan orogeny, the Levadio Shear Zone juxtaposed the deeper crustal rocks of the Mammola Paragneiss Unit with the upper crustal portion, represented by the Stilo–Pazzano Phyllite Unit (Festa et al. 2018; Tursi et al. 2020b). The mylonitic foliation of the Mammola Paragneiss Unit (Fig. 3a) developed during an extensional tectonic event, which triggered the exhumation of the related crustal level from ~ 30–35 km to ~ 10 km depth, where it was coupled to the upper crustal Stilo–Pazzano Phyllite Unit (Tursi et al. 2020b) (Fig. 3b). Sample MR21 (Tables 1, 2) from Tursi et al. (2020b) is considered here as representative of the mylonitic paragneisses of the Mammola Paragneiss Unit. The mineral assemblage of this rock is constituted by q + pl + bi + mu + g + chl + ilm ± ksp, with the main mylonitic foliation defined by fine-grained recrystallised quartz-feldspathic bands that alternate to mica-rich bands (Fig. 3b). Pre-kinematic garnet porphyroblasts are dispersed in the matrix and wrapped around by the quartz-feldspathic and mica-rich bands (Fig. 3b), with syn-kinematic chlorite that primarily grew within the garnet strain shadows, replacing garnet and biotite (Fig. 3b). Phase equilibrium results by Tursi et al. (2020b) have evidenced that the coupling between the Mammola Paragneiss Unit and the Stilo–Pazzano Phyllite

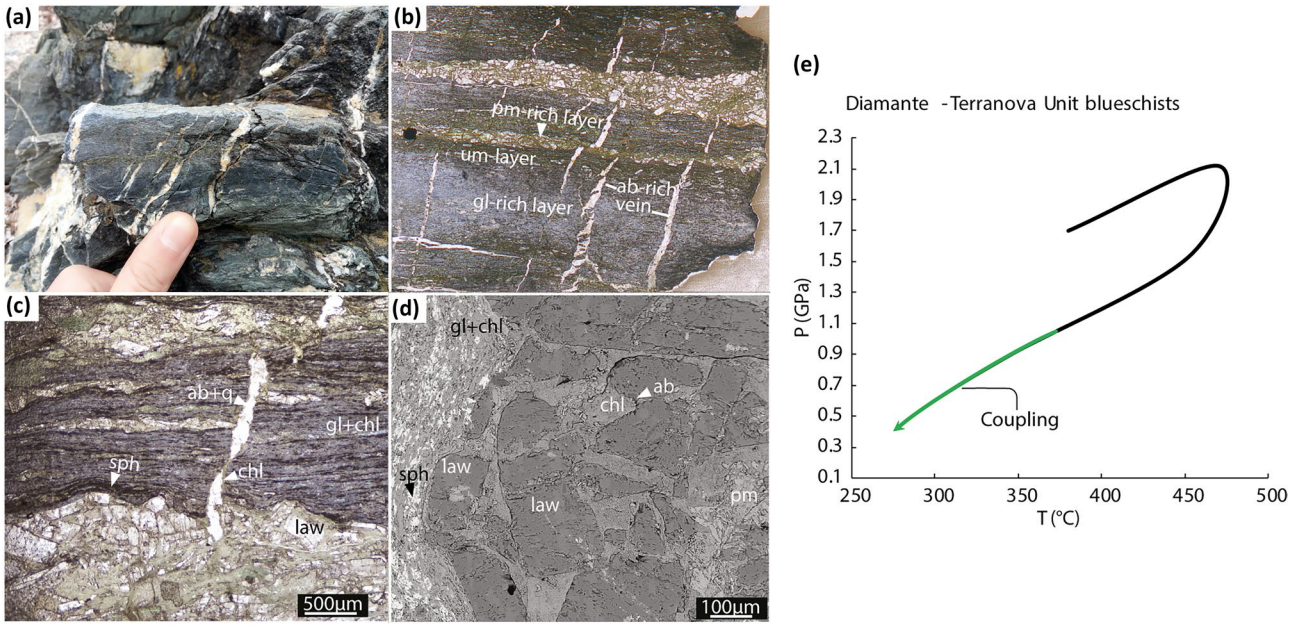

Fig. 2 (**a**) Detail of the Diamante–Terranova Unit mylonitic blueschists exposed at La Guardiola cliff, showing alternating bluish and greenish bands, the former crosscut by albite-rich veins. (**b**) Thin section scan (crossed polars) of sample DIA1a, highlighting the alternating glaucophane-rich bands and pumpellyite-rich bands, with the boundary commonly characterised by ultramylonitic (um) bands; the set of albite-rich veins can be also appreciated. (**c**) Microphotograph (crossed polars, sample DIA1a) showing the albite-rich veins connecting the pumpellyite-rich bands and crosscutting the glaucophane-rich ones. (**d**) SEM-BSE image showing the large lawsonite porphyroblasts overgrown by pumpellyite and chlorite in the pumpellyite-rich bands. (**e**) *P–T* path of the Diamante–Terranova Unit blueschists from Tursi et al. (2020a); the *P–T* conditions inferred for the coupling with the underlying carbonate rocks from the Lower Complex are highlighted in green. Figures (**a**)–(**d**) modified after Tursi et al. (2020a)

Unit (Fig. 3c) occurred under fluid-deficient conditions, despite the presence of syn-kinematic chlorite in the strain shadows of garnet porphyroblasts.

The Curinga–Girifalco Line

In the northern Serre Massif (Fig. 1d), the Castagna Unit, formerly part of the Variscan intermediate crust, under-thrusted the Sila and Serre Unit during the Alpine orogeny along the Curinga–Girifalco Line (Fig. 1d) (Brandt and Schenk 2020; Festa et al. 2020). The Curinga–Girifalco Line was consecutively re-activated under the extensional-dominating tectonics that took place from Late Eocene to Early Miocene (Festa et al. 2020). Tursi et al. (2021) highlighted variations in the mineral assemblage of the Castagna Unit's orthogneiss from the weakly-deformed host rock towards the shear zone (Fig. 4a). The primary difference between the weakly-deformed and mylonitic orthogneisses concerns the presence of garnet (Fig. 4b), as garnet is only present in the latter (Tursi et al. 2021). Sample VF77GR (Tables 1, 2) from Tursi et al. (2021) is here considered as representative of the mylonitic orthogneiss of the Castagna Unit. The mineral assemblage of this rock consists of q + ksp + pl + mu + bi + g + ep + sph, with fine-grained recrystallised quartz-feldspathic bands alternating with mica-rich ones (Fig. 4b, c). Quartz, plagioclase and K-feldspar porphyroclasts, up to one-millimetre in size, as well as sub-millimetre, pre-kinematic garnet porphyroblasts that host quartz, albite, white mica and titanite inclusions, are anastomosed by the main mylonitic foliation (Fig. 4b, c). After investigating the fluid-present/deficient conditions that

Table 1 Samples considered in this study; the mylonitic mineral assemblage, along with the metamorphic stage and the P–T conditions of equilibration during coupling are also reported

Sample	Reference	Rock type	Mylonitic mineral assemblage	Metamorphic stage	P–T conditions of coupling
DIA1a	Tursi et al. (2020a)	blueschist	gl + law + chl + pmp + q + sph + ab + ep	retrograde	0.6–1.1 GPa, 290–380 °C
MR21	Tursi et al. (2020b)	paragneiss	q + pl + bi + mu + g + chl + ilm + ksp	retrograde	0.3 GPa, 440–460 °C
VF77GR	Tursi et al. (2021)	orthogneiss	q + ksp + pl + mu + bi + g + ep + sph	prograde	0.7–0.95 GPa, 540–590 °C

Table 2 Bulk rock compositions (in wt.%) of mylonitic samples DIA1a (from Tursi et al. 2020a), MR21 (Tursi et al. 2020b) and VF77GR (Tursi et al. 2021)

Sample	H_2O/LOI	SiO_2	Al_2O_3	CaO	MgO	Fe_2O_3	K_2O	Na_2O	TiO_2	MnO	P_2O_5	Total
DIA1a	4.69	42.73	15.14	10.34	9.84	12.80	0.13	1.94	2.04	0.18	0.02	99.85
MR21	1.56	63.90	16.22	2.14	2.11	6.09	3.15	3.56	0.92	0.08	0.26	99.99
VF77GR	0.93	73.36	13.17	0.83	0.79	2.55	4.88	3.01	0.35	0.05	0.07	99.99

affected the orthogneisses, Tursi et al. (2021) imputed the stabilisation of garnet within the mylonitic orthogneisses during the prograde path (Fig. 4d) to the catalytic role exerted by aqueous fluids, though different degrees of fluid-saturation occurred in these rocks.

Methods and basic concepts

To investigate the possible occurrence in the study rocks of reaction products related to variations of chemical potentials during the mylonitic event, chemical potential diagrams were calculated using the software THERMOCALC v3.45 (Powell and Holland 1988) and the updated version of the internally consistent thermodynamic dataset ds62 (Holland and Powell 2011) (tc-ds63.txt, created on 05/01/2015). Activity-composition models for metabasite-forming minerals are from Green et al. (2016) while those for metapelite-forming minerals are from White et al. (2014). According to the simplified chemical system used in each case study, quartz, albite, anorthite, clinozoisite, Mg-pumpellyite, lawsonite and aqueous fluid were considered pure endmembers. Mineral abbreviations are from Holland and Powell (1998).

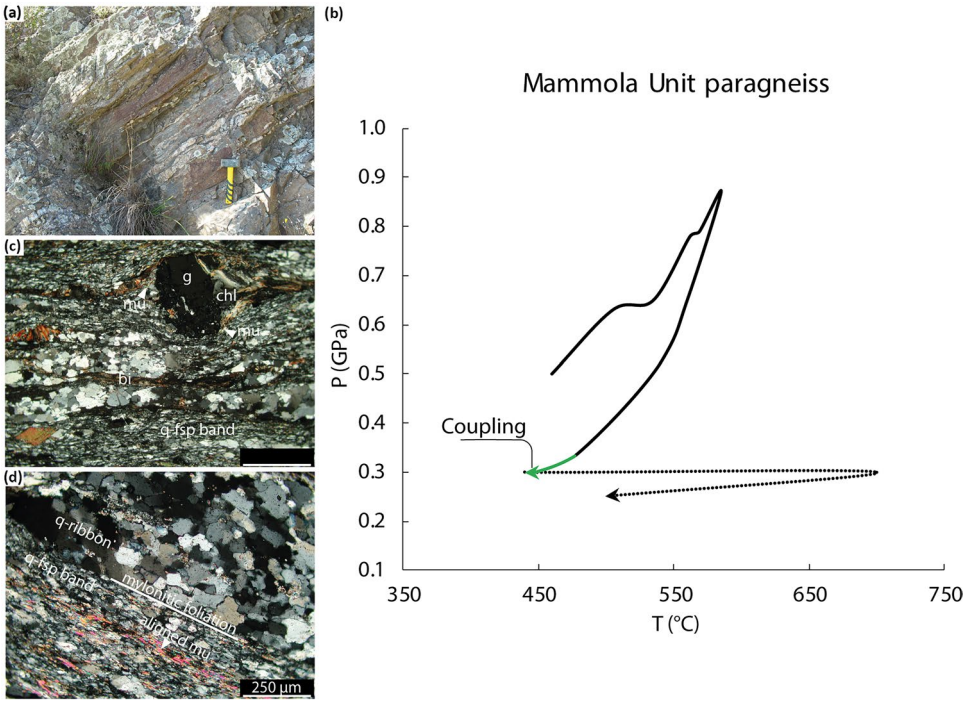

Fig. 3 (**a**) Detail of the Mammola Unit mylonitic paragneiss exposed along the Levadio Shear Zone (Festa et al. 2018), showing stretched and boudinaged leucocratic bands. (**b**) *P–T* path of the Mammola Unit paragneiss from Tursi et al. (2020b); the *P–T* conditions inferred for the coupling with the overlying Stilo–Pazzano Phyllite Unit is highlighted in green; the part of the path related to contact metamorphism is dotted (see Tursi et al. 2020b). (**c**) Microphotograph (crossed polars) of sample MR21, where it is illustrated the alternation of quartz-feldspathic and mica-rich bands, that anastomose a garnet porphyroblast with chlorite strain shadows; modified after Tursi et al. (2020b). (**d**) Detail of the alternation of quartz ribbons, quartz-feldspathic and tiny mica-rich bands in sample MR21, which define the main mylonitic foliation

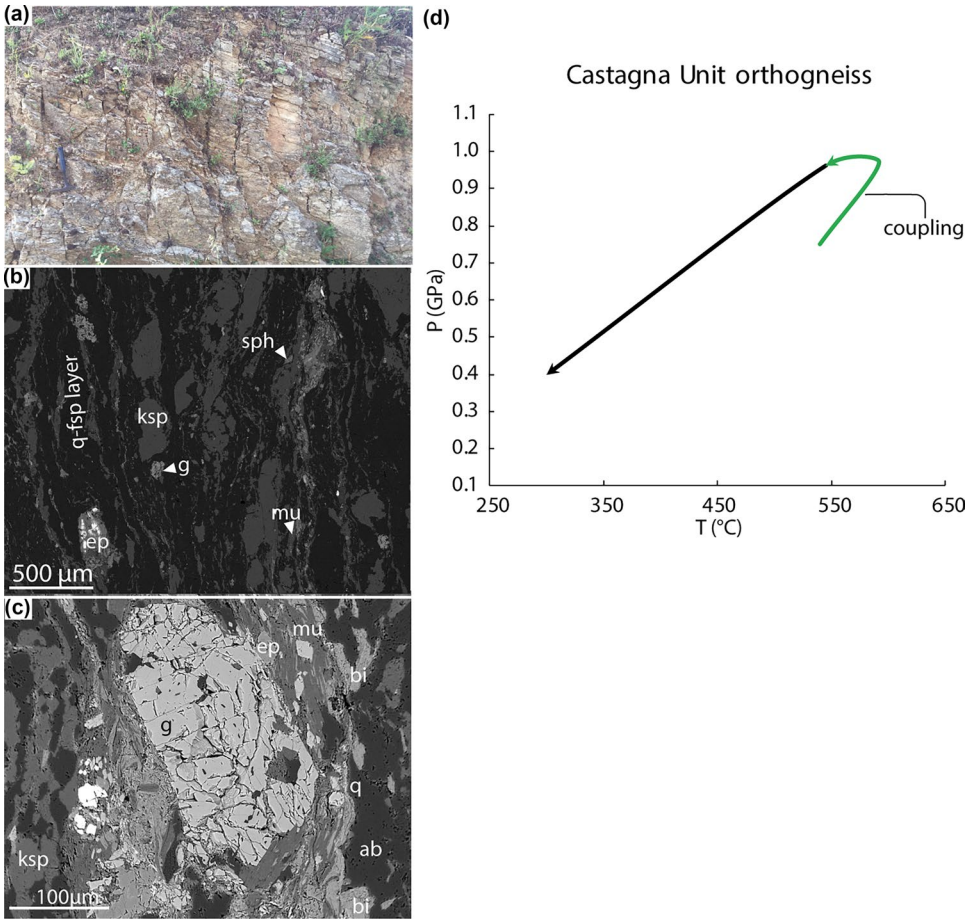

Fig. 4 (**a**) Outcrop of Castagna Unit mylonitic orthogneiss exposed along the eastern-branch of the Curinga–Girifalco Line (Festa et al. 2020), showing a marked mylonitic foliation (modified after Tursi et al. 2021). (**b**) SEM-BSE imaging of sample VF77GR highlighting the main mylonitic foliation defined by fine grain recrystallised quartzofeldspathic bands alternating with thin mica-rich ones both anastomosing quartz and K-feldspar porphyroclasts and garnets porphyroblasts. (**c**) SEM-BSE imaging of sample VF77GR showing alternating quartz-K-feldspar-albite and mica-rich bands, the latter anastomosing a garnet porphyroblast; note the presence of epidote in the mica-rich band. (**d**) *P*–*T* path of the Castagna Unit mylonitic orthogneiss from Tursi et al. (2021); the P–T conditions inferred for the coupling with the overlying Sila Unit is highlighted in green

Chemical potential diagrams and background theory

When considering a system undergoing changes, as in the case of a rock experiencing metamorphism, the thermodynamic variables describing the change are of two types: intensive (temperature, T, pressure, P, and the chemical potential μ_k of a component k) and extensive (entropy, S, volume, V, and the molar quantity n_k of a component k) (Powell et al. 2005; White et al. 2008). The intensive variables do not depend on the quantity of material concerned and are external, that is to say imposed on the system from the outside. When local equilibrium is achieved, the intensive variables have the same values in each point of the system (contact equilibrium), being equalised by thermal conduction (T), deformation (P), and elemental diffusion (μ_k) (other than infiltration). Extensive variables instead, have values that depend on the amount of material, whilst they are commonly considered in normalised form (Powell et al. 2005; White et al. 2008); they are internal to the system, in the sense that their evolution results from an adaptation of the system to the evolution of the intensive external variables. Intensive and extensive variables come in conjugate pairs, whose products (PV, TS, $\mu_k n_k$) are energy quantities. In phase diagrams, only one variable out of each conjugate pair can be considered; its choice depends on the efficacy of the variable in describing the examined process (Powell et al. 2005). Here, we mainly use μ_k-μ_l diagrams, which obey Schreinemakers' rules similarly to *P*–*T* petrogenetic grids (e.g. Zen 1974).

Korzhinskii (1959) first realised that metamorphic rocks commonly do not show complete equilibration, and that local equilibrium (mosaic equilibrium) is usual instead. The flattening of chemical potential gradients in high-grade metamorphic rocks was focussed on by White et al. (2008). Considering a "closed system", these authors highlighted that, during a metamorphic reaction due to P and T changes, the growth of new minerals occurs in order to eliminate chemical potential gradients set up in the rock between reactant minerals through diffusion of components.

In the case of mylonitic rocks, diffusion may be facilitated by strain (Hobbs and Ord 2017; Wheeler 2020), and chemical potential gradients can be easily eliminated as mineral reactions are favoured, although the overall effect on mineral equilibria may be of second-order (Powell et al. 2018). Likewise, even in ductile shear zones that behaved as

"closed system", the growth of new syn-kinematic minerals can be investigated considering the chemical potential μ_k of a component k, as the natural variable of the conjugate pair (μ_k, n_k). This approach is applied below to mylonitic rocks, in order to decipher their microstructures, the formation of reaction products and the survival of porphyroblasts during ductile shearing.

Chemical potential gradients in mylonitic rocks

Mylonitic blueschist of the Diamante–Terranova Unit

A banded mylonitic blueschist (sample DIA1a; Table 1) was investigated in relation to chemical potential gradients developed during the shearing event. According to Tursi et al. (2020a), different equilibria that consumed glaucophane and lawsonite and stabilised pumpellyite, chlorite, quartz and albite were responsible for the generation of the banded fabric, like:

$4tr + 64law = 36cz + 5ames + 42q + 94H_2O$ (E1);
$16tr + 112law = 11ames + 36mpm + 114q + 70H_2O$ (E2);
$17tr + 86law = 11clin + 30mpm + 95q + 40H_2O$ (E3);
$71gl + 80law = 19cumm + 15ames + 20mpm + 142ab + 82H2O$ (E4)

The main reaction responsible for the genesis of the banded fabric can be consequently written in the general form of:

$$\text{Glaucophane} + \text{Lawsonite} = \text{Chlorite} + \text{Pumpellyite} + \text{Quartz} + \text{Albite} + H_2O \quad (1)$$

The minimum number of components describing this reaction is six, i.e., NCMASH. Chemical potential relationships for reaction (1) were firstly investigated under fluid-present conditions, considering chlorite and quartz present in each stability field, as these minerals are in contact with all the minerals composing the assemblage. Considering that Al is less mobile than Na, Ca and Mg (e.g. Tursi et al. 2018, and references therein), the nature of the banded fabric was evaluated in the μCaO–μNa_2O and μCaO–μMgO space (Fig. 5a, b). Both grids show two points where the assemblages (i) law + mpm + ab and (ii) gl + ab + mpm are stable, accounting for the pumpellyite-rich and glaucophane-rich bands (Fig. 2). Accordingly, the mineral assemblage of the pumpellyite-rich bands can develop in response to small variations of μNa_2O and μMgO (Fig. 5a, b respectively). Therefore, assuming excess of fluid in the rock, the banded fabric of the sheared blueschists can be reproduced moving from the gl-field to the law + mpm + ab point, decreasing either μNa_2O or μMgO (Fig. 5a, b). Although H_2O is a perfectly mobile component, the banded fabric of the rock seems to be related to alternating fluid-present and fluid-deficient bands (Tursi et al. 2020a), thus recording μH_2O gradients. Hence, chemical potential relationships have been investigated in a 3D-space (Fig. 5c) to evaluate if gradients in the chemical potential of the fluid phase actually played a role in the banded fabric evolution (Fig. 2). In this case, H_2O cannot be assumed as an in-excess phase, so the chemical potential relationships have been investigated with respect to the fluid saturation surface, which occurs at μH_2O of -324.467 kJ.mol^{-1}. As shown in the 3D-sketch of Fig. 5c, the gl-law-mpm-ab invariant point occurs above the fluid saturation surface (i.e. μH_2O of -324.445 kJ.mol^{-1}) in the μCaO–μMgO–μH_2O 3D-space. Projecting from this point below the fluid saturation surface allows investigation of the assemblages (i) and (ii) with respect to μH_2O (Fig. 5c). To make these two assemblages invariants, μCaO was fixed at -754.47 kJ.mol^{-1} and the chemical potential relationships have been evaluated on the μMgO–μH_2O grid (Fig. 5d). The gl-mpm-ab invariant point occurs at slightly higher μMgO and lower μH_2O than the law-mpm-ab invariant point, respectively, the latter occurring close to the fluid saturation line (Fig. 5d). Consequently, for the μCaO considered, an increase of ~ 0.01 kJ.mol^{-1} of μH_2O and a decrease of ~ 0.01 kJ.mol^{-1} of μMgO is needed to move from the gl-mpm-ab point to the law-mpm-ab point at 0.92 GPa and 375.29 °C.

Mylonitic paragneiss of the Mammola Paragneiss Unit

To investigate the occurrence of chlorite under fluid-deficient conditions in the mylonitic paragneisses of the Mammola Paragneiss Unit (Fig. 3), I considered sample MR21 (Table 1). Chemical potential relationships were evaluated in the NCKFMASH model system, neglecting MnO, as it resulted mostly stored in garnet rather than in the other Mn-bearing minerals (e.g., chlorite and biotite), as well as TiO_2, because Ti-bearing minerals were not involved in chlorite formation (cf. Tursi et al. 2020b). Moreover, since Fe^{3+}-bearing minerals like epidote are not present in the mylonitic mineral assemblage, Fe_2O_3 can be excluded as a component, making $FeO_{tot} = FeO$.

To calculate chemical potential diagrams, a value for μAl_2O_3 of -1718.57 kJ.mol^{-1} was superimposed, assuming Al_2O_3 as immobile component. Biotite, quartz, plagioclase and albite are in contact with all the mineral phases in the assemblage of sample MR21 (Fig. 3c), so they can be assumed as present in each stability field. The presence of chlorite in the mylonitic paragneiss is predicted below

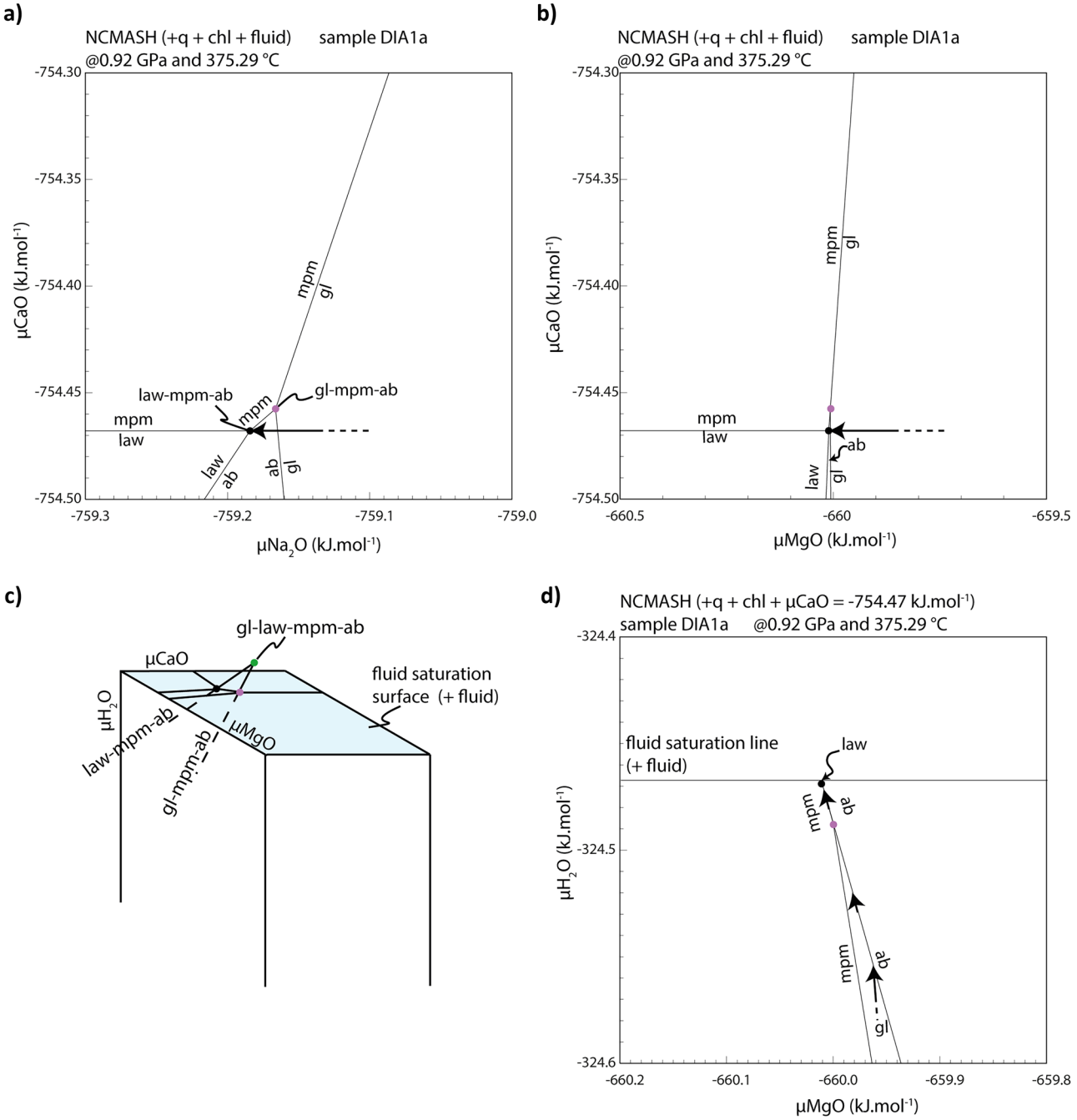

Fig. 5 (**a**, **b**) Chemical potential relationships in the Na_2O–CaO–MgO–Al_2O_3–SiO_2–H_2O (NCMASH) model system calculated at 0.92 GPa and 375.29 °C; the phase relations for reaction (1) are shown in the μCaO–μNa_2O space (**a**) and the μCaO–μMgO space (**b**), with the two invariant points highlighted (law-mpm-ab point, black circle; gl-mpm-ab point, purple circle). (**c**) Phase relations in the μCaO–μMgO–μH_2O 3D-space; the dashed lines below the fluid saturation surface (pale blue surface) are projections that start above this surface (solid lines), from the gl-law-mpm-ab invariant point (green circle), and transect the fluid saturation surface through the two points law-mpm-ab and gl-mpm-ab of Fig. 5b. (**d**) Chemical potential relationships in the Na_2O–CaO–MgO–Al_2O_3–SiO_2–H_2O (NCMASH) model system with quartz and chlorite in excess calculated at 0.92 GPa and 375.29 °C; the phase relations for reaction (1) are shown in the μH_2O–μMgO space. The diffusion paths (black arrows) from the gl-field to the law-mpm-ab point (black circle) are highlighted in (**a**), (**b**) and (**d**)

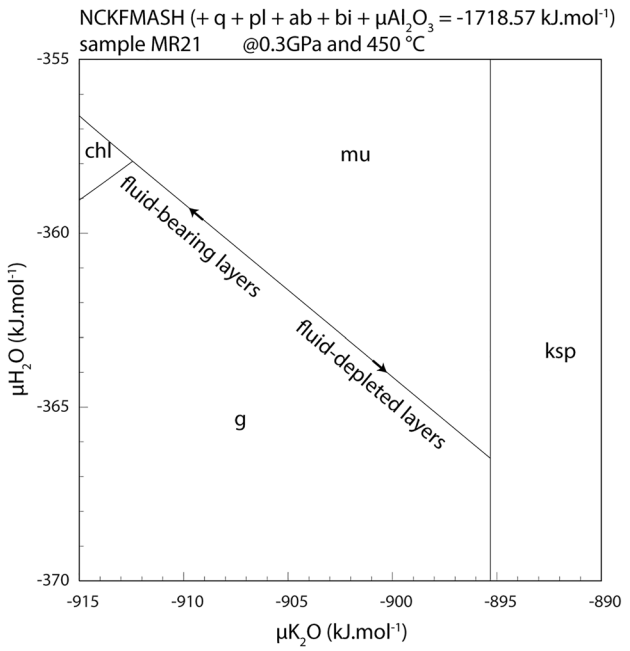

Fig. 6 Chemical potential relationships in the Na_2O–CaO–K_2O–FeO–MgO–Al_2O_3–SiO_2–H_2O (NCKFMASH) model system calculated at 0.3 GPa and 450 °C; the phase relations for reaction (2) are shown in the μH_2O–μK_2O space. The diffusion paths (black arrows) from the g-mu univariant curve to the g-mu-chl and g-mu-ksp points are highlighted

the fluid saturation line ($\mu H_2O = -345.43$ kJ.mol^{-1}) in the μH_2O–μK_2O grid (Fig. 6), with chlorite formation related to the following general reaction, as suggested by its interposition between garnet and biotite in the garnet strain shadows (Fig. 3):

$$\text{Garnet} + \text{Biotite} + H_2O = \text{Chlorite} + \text{Muscovite} + \text{Quartz} \quad (2)$$

Two invariant points occur in the μH_2O–μK_2O grid: the g-mu-chl point occurs at higher μH_2O and lower μK_2O with respect to the g-mu-ksp point. Hence, moving along the g-mu curve, chlorite is stabilised where high μH_2O (≥ -358 kJ.mol^{-1}) and low μK_2O (≤ -913 kJ.mol^{-1}). On the other hand, K-feldspar is stable at low μH_2O (≤ -367 kJ.mol^{-1}) and high μK_2O (≥ -895 kJ.mol^{-1}).

Mylonitic orthogneiss of the Castagna Unit

Garnet formation related to chemical potential gradients of the fluid within the mylonitic orthogneisses of the Castagna Unit is investigated for sample VF77GR (Table 1). Considering the different equilibria described by Tursi et al. (2021) for sample VF77GR (Table 1), the formation of garnet in this mylonitic orthogneiss is primarily linked to the following equilibria:

$$6cz = 2gr + 5an + ma + 2H_2O \text{ (E5)};$$
$$mu + Mn\text{-}bi + 3q = spss + 2san + 2H_2O \text{ (E6)};$$
$$mu + 2phl + 6q = py + 3cel \text{ (E7)};$$
$$mu + 2ann + 6q = alm + 3fcel \text{ (E8)};$$

Hence, the general garnet-forming reaction can be written in the form:

$$\text{Biotite} + \text{Clinozoisite}(+\text{Muscovite} + \text{Quartz}) = \text{Garnet} + \text{Anorthite} + \text{K} - \text{Feldspar} + \text{Phengite} + H_2O \quad (3)$$

Accordingly, chemical potential relationships were investigated in the 7-component, CKFMASH model system, with quartz, muscovite and K-feldspar assumed as present in each stability field. To calculate chemical potential diagrams, a value of μMgO of -685.00 kJ.mol^{-1} was fixed. This value was calculated at 0.75 GPa and 570 °C, considering the intersecting area of garnet's core isopleths calculated by Tursi et al. (2021) for this sample. As H_2O was in insufficient amount to saturate this rock (cf. Tursi et al. 2021), chemical potential relationships in the μH_2O–μCaO space at a fixed temperature of 570 °C, and at two reference pressures of 0.75 GPa and 0.95 GPa were considered (Fig. 7a), corresponding to the equilibration of garnet core and garnet rim, respectively (Tursi et al. 2021). At 0.75 GPa, there are two invariant points, namely (i) g-bi-cz and (ii) an-bi-cz. These two assemblages occur at different μH_2O, with the g-bi-cz point closer to the fluid saturation surface and at higher μCaO with respect to the an-bi-cz point (Fig. 7a). Hence, a diffusion path along the bi-cz curve to the g-bi-cz invariant point can be inferred, with garnet starting to grow within sites of high μH_2O and μCaO (Fig. 7a). At 0.95 GPa, the bi-cz curve splits the μH_2O–μCaO space, and only the bi-an-cz invariant point occurs, but at lower μH_2O than that at 0.75 GPa (Fig. 7a). Moving towards higher μH_2O along the bi-cz univariant curve, the fluid saturation surface is crossed at -348.04 kJ.mol^{-1} (Fig. 7a). If H_2O saturation is considered at 0.95 GPa and 570 °C, the chemical potential relations in the μMgO–μCaO space (Fig. 7b) show that the g-bi-cz invariant point is encountered and diopsidic clinopyroxene may form at higher μMgO with respect to this point. Here, biotite has a small stability field, as it breaks down to form either garnet or diopside, which occur in association with excess phases according to the particular chemical potential gradient established in the rock (Fig. 7b).

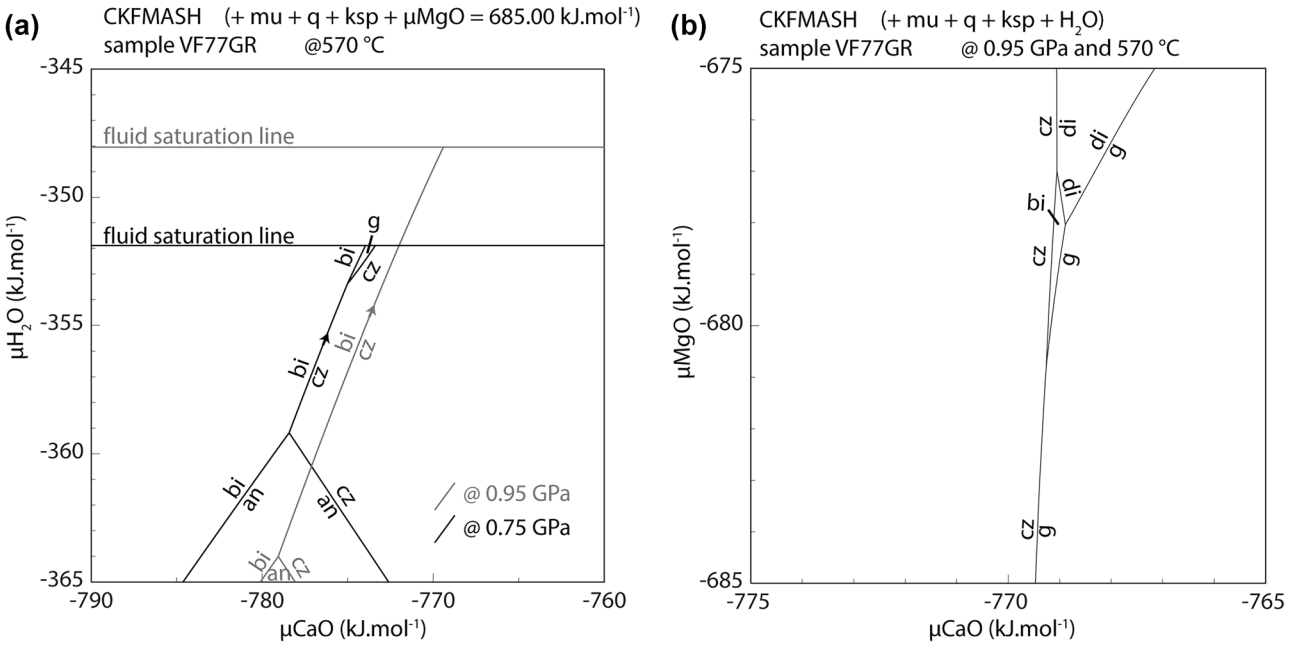

Fig. 7 (**a**) Chemical potential relationships in the CaO–K_2O–FeO–MgO–Al_2O_3–SiO_2–H_2O (CKFMASH) model system calculated at 570 °C and 0.75 GPa (black lines) and 0.95 GPa (grey lines); the phase relations for reaction (3) (see text for details) are shown in the μH_2O–μCaO space. The diffusion paths (black and grey arrows) along the bi-cz univariant curve towards higher μH_2O are highlighted. (**b**) Chemical potential relationships in the μMgO–μCaO space calculated at 570 °C and 0.95 GPa

Discussion

The results shown above highlight the usefulness of chemical potential diagrams to deciphering the petrologic nature of syn-kinematic reaction products developed in mylonitic rocks that behaved as "closed system", extending their use beyond the interpretation of diffusion-driven high-grade reaction textures (Baldwin et al. 2005, 2015; White et al. 2008; White and Powell 2010, 2011; Schorn and Diener 2017; Schorn et al. 2020) or mineral assemblage variations related to fluid infiltration (Goncalves et al. 2012; Evans et al. 2013; Tumiati et al. 2015). In fact, considering the Diamante–Terranova Unit mylonitic blueschist from La Guardiola Shear Zone, the occurrence of chlorite, pumpellyite, albite and quartz as syn-kinematic reaction products in narrow zones, is related to the onset of chemical potential gradients during ductile shearing (Fig. 5). In particular, a diffusion path from the gl-field to the law-mpm-ab invariant point, moving along the gl-ab and mpm-ab univariant curves (Fig. 5d), occurred in relation to chemical potential gradients, especially in μH_2O. This diffusion path (Fig. 5d) allows to refining the schematic evolution of the banded fabric of the mylonitic blueschists (Tursi et al. 2020a), as the pumpellyite-rich bands developed in response to locally higher μH_2O than in the glaucophane-rich bands, favouring lawsonite preservation therein. The pumpellyite-rich bands continued deforming in a ductile way during exhumation, while the glaucophane-rich bands behaved brittlely (Tursi et al. 2020a), as suggested by the textural relationships between the albite-rich veins and the glaucophane- and pumpellyite-rich bands, respectively (see Tursi et al. 2020a). This indicates that pumpellyite was more ductile than glaucophane during the shearing event that characterised the final stage of exhumation of the Diamante–Terranova blueschist from ~ 1.1 GPa and 380 °C to 0.7 GPa and 290 °C (Tursi et al. 2020a), in particular at the *P*–*T* conditions of veins development. Hence, the formation of reaction products allowed sustaining ductile shearing, in line with the experimental results by Holyoke and Tullis (2006a), with the reaction products that formed in narrow zones where μH_2O is locally higher than in the surroundings, which is compatible with narrowing of ductile shear zones when fluid in the system is limited (Menegon et al. 2017; Kaatz et al. 2021).

Another aspect of the setup of μH_2O gradients in rocks during deformation deserving attention is that relict anhydrous reactant minerals survive metastably in sites where μH_2O is lower, while the product minerals preferentially form where μH_2O is higher (Figs. 5–7). This supports the results of Rubie (1986) and Guiraud et al. (2001) about enhanced reaction kinetics under fluid-present conditions, and suggests that delayed nucleation kinetic in metamorphic rocks is primarily imputed to overall fluid-deficient conditions attained during their evolution, with μH_2O not high enough in each point of the

rock to promote the growth of new minerals as *P* and *T* change. Therefore, under high-strain ductile deformation, if high fluid influx occur, mineral reactions are favoured and brought at completion (e.g. Tursi et al. 2018), and not delayed (Rubie 1998). This can be appreciated in the Mammola Unit mylonitic paragneiss, where the formation of chlorite through reaction (2) as syn-kinematic product requires fluid, in apparent contrast with the presence of pre-kinematic garnet porphyroblasts surviving metastably (Fig. 3). Even in this case, the fluid was internally provided during exhumation and shearing, after the paragneiss experienced peak metamorphic conditions (Fig. 3). Considered the mineral assemblage of the investigated sample (MR21; Table 1), one of the reactions releasing fluid during decompression that can be invoked is the one breaking down white mica (Massonne and Schreyer 1987):

$$\text{Phengite} = \text{Biotite} + \text{K} - \text{feldspar} + \text{Quartz} + \text{H}_2\text{O} \quad (4)$$

Therefore, the fluid released by reaction (4) was likely channelled during shearing, favouring the onset of gradients in μH_2O and chlorite stabilisation within opportune sites where nutrients for its growth were available, e.g., at garnet–biotite grain boundaries (Fig. 3). Consequently, reaction (2) consumed the fluid provided by reaction (4) in the system, promoting fluid-deficient conditions during retrogression and shearing (cf. Tursi et al., 2020b), which allowed the preservation of pre-kinematic garnet porphyroblasts (Fig. 3). In fact, whilst exhumation through shearing could be faster than reaction kinetics, allowing time-dependent garnet preservation, diffusion and mineral reactions may be promoted by deformation (Holyoke and Tullis 2006a, b). This, therefore, makes the kinetic effect irrelevant for the preservation of relict garnet porphyroblasts.

As regards the banded fabric of the mylonitic paragneiss (Fig. 3b), the μH_2O–μK_2O grid of Fig. 6 suggests that gradients in μK_2O, in addition to those in μH_2O, occurred between the quartz-feldspathic and mica-rich bands (e.g., sample MR21 in Fig. 3), due to simultaneous consumption of white mica through the reversal reaction (2). This resulted in μK_2O higher in quartz-feldspathic bands than in mica-rich ones (e.g., sample MR21 in Fig. 3), favouring the development of the banded fabric in the rock (Fig. 3b).

Fluid storage during ductile shearing was also revealed by sample VF77GR of Castagna Unit mylonitic orthogneiss (Fig. 4), which followed a fluid-conservative trajectory during prograde Alpine metamorphism, starting from fluid-present conditions (Tursi et al. 2021). The fluid was provided internally by the breakdown of biotite and clinozoisite through reaction (3), and, as shown in the μH_2O–μCaO grid of Fig. 7a, garnet, the reaction product, grew in high-μH_2O conditions, despite garnet is normally anhydrous. Although the onset of reaction was probably favoured by deformation in the shear zone (Hobbs and Ord 2017; Wheeler 2020), this μH_2O–μCaO grid illustrates that garnet nucleation was actually enhanced in this rock by the catalytic role of fluid. During exhumation, on the other hand, garnet was preserved, favoured by overall fluid-deficient conditions during the re-activation of the Curinga–Girifalco Line (Tursi et al. 2021).

The results obtained by the analysis of chemical potentials in the mylonitic rocks examined highlight how syn-kinematic minerals form as product of mineral reactions even under overall fluid-deficient conditions, within higher μH_2O conditions than the surrounding (Figs. 5–7). These results appear in line with those of Powell et al. (2018), suggesting that strain plays only a second-order effect on mineral equilibria, while the system primarily adjusts with respect to variations of *P, T* and μ. In addition, nucleation of new, syn-kinematic minerals allows removal of stress in the deforming rock, as evidenced by the experimental results of Holyoke and Tullis (2006a, b), with the mylonite being rheologically weaker than the wall rocks due to the presence of fluid released by devolatilization reactions.

Despite investigation of rock texture and reaction microstructures in metamorphic rocks through chemical potential diagrams is one of our most advanced and powerful approach to understanding the evolution of metamorphic systems (Powell et al. 2019), some limitations occur due to common underlying assumptions when modelling natural processes. In this case, a possible effect on mineral stability could be related to the lacking of models for minor components in the current thermodynamic datasets, like Cl in chlorite, micas and amphiboles (e.g. Kullerud 1995, 1996; Barnes et al. 2019). In particular, the chemistry of the fluid released by reactions that involve the breakdown of these minerals may be affected by variation in the chloride content. Chloride-rich fluids, depending of their cation load, can affect the chemistry of minerals, like plagioclase or Fe–Mg silicates, in equilibrium with the fluid (e.g. Yardley and Bodnar 2014, and references therein). However, chlorine concentration is commonly low in the above mentioned Cl-bearing minerals and large fluid influx are needed to make efficient the fluid-rock interaction (Manning 2018; Tursi et al. 2018); hence, the results of this study appear robust as overall fluid-deficient conditions affected the examined mylonites.

Concluding remarks

The present approach is useful to decipher the mineral assemblages characterising ductile shear zones, challenging the common belief that these represent preferential channels for fluids in the Earth's crust. Although the selected case studies are localised within the Calabria polymetamorphic terrane, the following conclusions result generally applicable to the broad context of ductile shear zones, turning useful to understand their rheology, fabric and reaction history, as outlined below:

(i) the investigated mylonites consumed their OH-bearing minerals either during under-thrusting or exhumation accompanied by extensional tectonics;
(ii) whether the shear zone developed during prograde or retrograde metamorphism, the release of fluid allowed the formation of new, syn-kinematic minerals within sites where the fluid saturation was approached;
(iii) as a consequence of the channelling of the fluid released by the breakdown of OH-bearing minerals, the ductile sheared rock is characterised by fluid-deficient bands (e.g. quartz-feldspathic) alternating to fluid-present bands (e.g. mica-rich);
(iv) mylonites preserving anhydrous pre-kinematic porphyroblasts and/or porphyroclasts developed under overall fluid-deficient conditions with fluid-bearing conditions affecting only local sites;
(v) during shearing, the breakdown of hydrous minerals favours the growth of new minerals (reaction products) within sites of high μH_2O. At the same time, it can be inferred that the fluid released in the system promotes deformation via reaction-induced rheological weakening, giving rise to a cascade effect.

Acknowledgements I am grateful to Alfredo Caggianelli, Vincenzo Festa and Richard Spiess for exchanging valuable scientific opinions and encouraging me in my research. Gaston Godard, an anonymous reviewer and the editor S.W. Faryad are thanked for their constructive comments and criticism, which improved the quality of the present manuscript. The JEO assistant Lhiric Agoyaoy is thanked for his editorial handling of the manuscript.

Funding Open access funding provided by Università degli Studi di Bari Aldo Moro within the CRUI-CARE Agreement.

References

Baldwin JA, Powell R, Brown M et al (2005) Modelling of mineral equilibria in ultrahigh-temperature metamorphic rocks from the Anápolis-Itauçu Complex, central Brazil. J Metamorph Geol 23:511–531. https://doi.org/10.1111/j.1525-1314.2005.00591.x

Baldwin JA, Powell R, White RW, Štípská P (2015) Using calculated chemical potential relationships to account for replacement of kyanite by symplectite in high pressure granulites. J Metamorph Geol 33:311–330. https://doi.org/10.1111/jmg.12122

Barnes JD, Penniston-Dorland SC, Bebout GE et al (2019) Chlorine and lithium behavior in metasedimentary rocks during prograde metamorphism: A comparative study of exhumed subduction complexes (Catalina Schist and Schistes Lustrés). Lithos 336–337:40–53. https://doi.org/10.1016/j.lithos.2019.03.028

Bell TH, Cuff C (1989) Dissolution, solution transfer, diffusion versus fluid flow and volume loss during deformation/metamorphism. J Metamorph Geol 7:425–447. https://doi.org/10.1111/j.1525-1314.1989.tb00607.x

Bell TH, Hayward N (1991) Episodic metamorphic reactions during orogenesis: the control of deformation partitioning on reaction sites and reaction duration. J Metamorph Geol 9:619–640. https://doi.org/10.1111/j.1525-1314.1991.tb00552.x

Brandt S, Schenk V (2020) Metamorphic response to Alpine thrusting of a crustal-scale basement nappe in southern Calabria (Italy). J Petrol. https://doi.org/10.1093/petrology/egaa063

Brodie KH, Rutter EH (1987) The role of transiently fine-grained reaction products in syntectonic metamorphism: natural and experimental examples. Can J Earth Sci. https://doi.org/10.1139/e87-054

Carminati E, Doglioni C (2012) Alps vs. Apennines: The paradigm of a tectonically asymmetric Earth. Earth-Science Rev 112:67–96. https://doi.org/10.1016/j.earscirev.2012.02.004

de Ronde AA, Stünitz H, Tullis J, Heilbronner R (2005) Reaction-induced weakening of plagioclase-olivine composites. Tectonophysics 409:85–106. https://doi.org/10.1016/j.tecto.2005.08.008

Etheridge MA, Wall VJ, Vernon RH (1983) The role of the fluid phase during regional metamorphism and deformation. J Metamorph Geol 1:205–236

Etheridge MA, Wall VJ, Cox SF (1984) High Fluid Pressures during Regional Metamorphism and Deformation: Implications for Mass Transport and Deformation Mechanisms 89:4344–4358

Evans KA, Powell R, Frost BR (2013) Using equilibrium thermodynamics in the study of metasomatic alteration, illustrated by an application to serpentinites. Lithos 168–169:67–84. https://doi.org/10.1016/j.lithos.2013.01.016

Fedele L, Tramparulo FDA, Vitale S et al (2018) Petrogenesis and deformation history of the lawsonite-bearing blueschist facies metabasalts of the Diamante-Terranova oceanic unit (southern Italy). J Metamorph Geol 36:691–714. https://doi.org/10.1111/jmg.12303

Festa V, Caggianelli A, Kruhl JH et al (2006) Late-Hercynian shearing during crystallization of granitoid magmas (Sila massif, southern Italy): Regional implications. Geodin Acta 19:185–195. https://doi.org/10.3166/ga.19.185-195

Festa V, Cicala M, Tursi F (2020) The Curinga-Girifalco Line in the framework of the tectonic evolution of the remnant Alpine chain in Calabria (southern Italy). Int J Earth Sci 109:2583–2598. https://doi.org/10.1007/s00531-020-01918-5

Festa V, Messina A, Paglionico A et al (2004) Pre-Triassic history recorded in the Calabria-Peloritani segment of the Alpine chain, southern Italy. An Overview Period Di Mineral 73:57–71

Festa V, Tursi F, Caggianelli A, Spiess R (2018) The tectono-magmatic setting of the Hercynian upper continental crust exposed in Calabria (Italy) as revealed by the 1:10,000 structural-geological map of the Levadio stream area. Ital J Geosci 137:165–174. https://doi.org/10.3301/IJG.2018.03

Fornelli A, Festa V, Micheletti F et al (2020) Building an orogen: Review of U-Pb zircon ages from the Calabria-Peloritani terrane to constrain the timing of the southern variscan belt. Minerals 10:1–29.https://doi.org/10.3390/min10110944

Goncalves P, Oliot E, Marquer D, Connolly JAD (2012) Role of chemical processes on shear zone formation: An example from the grimsel metagranodiorite (Aar massif, Central Alps). J Metamorph Geol 30:703–722. https://doi.org/10.1111/j.1525-1314.2012.00991.x

Graessner T, Schenk V (1999) Low-pressure metamorphism of Palaeozoic pelites in the Aspromonte, southern Calabria: Constraints for the thermal evolution in the Calabrian crustal cross-section during the Hercynian orogeny. J Metamorph Geol 17:157–172.https://doi.org/10.1046/j.1525-1314.1999.00188.x

Green ECR, White RW, Diener JFA et al (2016) Activity-composition relations for the calculation of partial melting equilibria in metabasic rocks. J Metamorph Geol 34:845–869. https://doi.org/10.1111/jmg.12211

Guiraud M, Powell R, Rebay G (2001) H2O in metamorphism and unexpected behaviour in the preservation of metamorphic mineral assemblages. J Metamorph Geol 445–454. https://doi.org/10.1046/j.0263-4929.2001.00320.x

Hentschel F, Janots E, Trepmann CA et al (2020) Corona formation around monazite and xenotime during greenschist-facies metamorphism and deformation. Eur J Mineral 32:521–544. https://doi.org/10.5194/ejm-32-521-2020

Hobbs BE, Ord A (2017) Pressure and equilibrium in deforming rocks. J Metamorph Geol 35:967–982. https://doi.org/10.1111/jmg.12263

Holland TJB, Powell R (2011) An improved and extended internally consistent thermodynamic dataset for phases of petrological interest, involving a new equation of state for solids. J Metamorph Geol 29:333–383. https://doi.org/10.1111/j.1525-1314.2010.00923.x

Holland TJB, Powell R (1998) An internally consistent thermodynamic data set for phases of petrological interest. J Metamorph Geol 16:309–343. https://doi.org/10.1111/j.1525-1314.1998.00140.x

Holyoke CW, Tullis J (2006a) The interaction between reaction and deformation: An experimental study using a biotite + plagioclase + quartz gneiss. J Metamorph Geol 24:743–762. https://doi.org/10.1111/j.1525-1314.2006.00666.x

Holyoke CW, Tullis J (2006b) Formation and maintenance of shear zones. Geology 34:105–108. https://doi.org/10.1130/G22116.1

Iannace A, Reddy SM, Bonardi G et al (2007) The carbonate tectonic units of northern Calabria (Italy): a record of Apulian palaeomargin evolution and Miocene convergence, continental crust subduction, and exhumation of HP–LT rocks. J Geol Soc London 164:1165–1186. https://doi.org/10.1144/0016-76492007-017

Kaatz L, Zertani S, Moulas E et al (2021) Widening of hydrous shear zones during incipient eclogitization of metastable dry and rigid lower crust – Holsnøy Western Norway Tectonics 1–19. https://doi.org/10.1029/2020tc006572

Keller LM, Abart R, Stünitz H, De Capitani C (2004) Deformation, mass transfer and mineral reactions in an eclogite facies shear zone in a polymetamorphic metapelite (Monte Rosa nappe, western Alps). J Metamorph Geol 22:97–118. https://doi.org/10.1111/j.1525-1314.2004.00500.x

Korzhinskii DS (1959) Physicochemical Basis of the Analysis of the Paragenesis of Minerals. Mineral Mag 32:142

Kullerud K (1995) Chlorine, titanium and barium-rich biotites: factors controlling biotite composition and the implications for garnet-biotite geothermometry. Contrib to Mineral Petrol 120:42–59. https://doi.org/10.1007/BF00311007

Kullerud K (1996) Chlorine-rich amphiboles: interplay between amphibole composition and an evolving fluid. Eur J Mineral 8:355–370. https://doi.org/10.1127/ejm/8/2/0355

Langone A, Caggianelli A, Festa V, Prosser G (2014) Time Constraints on the Building of the Serre Batholith: Consequences for the Thermal Evolution of the Hercynian Continental Crust Exposed in Calabria (Southern Italy). J Geol 122:183–199. https://doi.org/10.1086/675227

Liberi F, Morten L, Piluso E (2006) Geodynamic significance of ophiolites within the Calabrian Arc. Isl Arc 15:26–43. https://doi.org/10.1111/j.1440-1738.2006.00520.x

Liotta D, Festa V, Caggianelli A et al (2004) Mid-crustal shear zone evolution in a syn-tectonic late Hercynian granitoid (Sila Massif, Calabria, southern Italy). Int J Earth Sci 93:400–413. https://doi.org/10.1007/s00531-004-0385-8

Manning CE (2018) Fluids of the Lower Crust: Deep Is Different. Annu Rev Earth Planet Sci 46:67–97. https://doi.org/10.1146/annurev-earth-060614

Massonne HJ, Schreyer W (1987) Phengite geobarometry based on the limiting assemblage with K-feldspar, phlogopite, and quartz. Contrib to Mineral Petrol 96:212–224. https://doi.org/10.1007/BF00375235

Menegon L, Pennacchioni G, Malaspina N et al (2017) Earthquakes as Precursors of Ductile Shear Zones in the Dry and Strong Lower Crust. Geochemistry, Geophys Geosystems 18:4356–4374. https://doi.org/10.1002/2017GC007189

Ortolano G, Visalli R, Fazio E et al (2020) Tectono-metamorphic evolution of the Calabria continental lower crust: the case of the Sila Piccola Massif. Int J Earth Sci 1–25. https://doi.org/10.1007/s00531-020-01873-1

Pennacchioni G, Cesare B (1997) Ductile-brittle transition in pre-Alpine amphibolite facies mylonites during evolution from water-present to water-deficient conditions (Mont Mary nappe, Italian Western Alps). J Metamorph Geol 15:777–791. https://doi.org/10.1111/j.1525-1314.1997.00055.x

Powell R, Evans KA, Green ECR, White RW (2018) On equilibrium in non-hydrostatic metamorphic systems. J Metamorph Geol 36:419–438.https://doi.org/10.1111/jmg.12298

Powell R, Evans KA, Green ECR, White RW (2019) The truth and beauty of chemical potentials. J Metamorph Geol 37:1007–1019. https://doi.org/10.1111/jmg.12484

Powell R, Guiraud M, White RW (2005) Truth and beauty in metamorphic phase-equilibria: Conjugate variables and phase diagrams. Can Mineral 43:21–33. https://doi.org/10.2113/gscanmin.43.1.21

Powell R, Holland TJB (1988) A internally consistent thermodynamic dataset with uncertainties and correlation: 3 Application to geobarometry, worked examples and a computer program. J Metamorph Geol 6:173–204

Prosser G, Caggianelli A, Rottura A, Del Moro A (2003) Strain localisation driven by marble layers: The Palmi shear zone (Calabria-Peloritani terrane, Southern Italy). GeoActa 2:155–166

Regenauer-Lieb K, Hobbs B, Ord A et al (2009) Deformation with coupled chemical diffusion. Phys Earth Planet Inter 172:43–54. https://doi.org/10.1016/j.pepi.2008.08.013

Rubie DC (1998) Disequilibrium during metamorphism: the role of nucleation kinetics. Geol Soc Spec Publ 138:199–214. https://doi.org/10.1144/GSL.SP.1996.138.01.12

Rubie DC (1986) The catalysis of mineral reactions by water and restrictions on the presence of aqueous fluid during

metamorphism. Mineral Mag 50:399–415. https://doi.org/10.1180/minmag.1986.050.357.05
Schenk V (1980) U-Pb and Rb-Sr radiometric dates and their correlation with metamorphic events in the granulite-facies basement of the Serre, Southern Calabria (Italy). Contrib to Mineral Petrol 73:23–38. https://doi.org/10.1007/BF00376258
Schorn S, Diener JFA (2017) Details of the gabbro-to-eclogite transition determined from microtextures and calculated chemical potential relationships. J Metamorph Geol 35:55–75. https://doi.org/10.1111/jmg.12220
Schorn S, Diener JFA, Sorger D, Clark C (2020) The contribution of charnockite magmatism to achieve near-ultrahigh temperatures in the Namaqua-Natal Metamorphic Province South Africa Lithos 368–369. https://doi.org/10.1016/j.lithos.2020.105585
Tumiati S, Godard G, Martin S et al (2015) Ultra-oxidized rocks in subduction mélanges? Decoupling between oxygen fugacity and oxygen availability in a Mn-rich metasomatic environment. Lithos 226:116–130. https://doi.org/10.1016/j.lithos.2014.12.008
Tursi F, Acquafredda P, Festa V et al (2021) What can high-P sheared orthogneisses tell us? An example from the Curinga-Girifalco Line (Calabria, southern Italy). J Metamorph Geol 39:919–944. https://doi.org/10.1111/jmg.12596
Tursi F, Bianco C, Brogi A et al (2020a) Cold subduction zone in northern Calabria (Italy) revealed by lawsonite–clinopyroxene blueschists. J Metamorph Geol 38:451–469. https://doi.org/10.1111/jmg.12528
Tursi F, Festa V, Fornelli A et al (2018) Syn-shearing mobility of major elements in ductile shear zones : state of the art for felsic deformed protoliths. Period Di Mineral 87:289–308. https://doi.org/10.2451/2018PM811
Tursi F, Spiess R, Festa V, Fregola RA (2020b) Hercynian subduction-related processes within the metamorphic continental crust in Calabria (southern Italy). J Metamorph Geol 38:771–793. https://doi.org/10.1111/jmg.12537
Wheeler J (2014) Dramatic effects of stress on metamorphic reactions. Geology 42:647–650. https://doi.org/10.1130/G35718.1
Wheeler J (2020) A unifying basis for the interplay of stress and chemical processes in the Earth: support from diverse experiments. Contrib to Mineral Petrol 175:1–27. https://doi.org/10.1007/s00410-020-01750-9
White RW, Powell R (2010) Retrograde melt-residue interaction and the formation of near-anhydrous leucosomes in migmatites. J Metamorph Geol 28:579–597. https://doi.org/10.1111/j.1525-1314.2010.00881.x
White RW, Powell R (2011) On the interpretation of retrograde reaction textures in granulite facies rocks. J Metamorph Geol 29:131–149. https://doi.org/10.1111/j.1525-1314.2010.00905.x
White RW, Powell R, Baldwin JA (2008) Calculated phase equilibria involving chemical potentials to investigate the textural evolution of metamorphic rocks. J Metamorph Geol 26:181–198. https://doi.org/10.1111/j.1525-1314.2008.00764.x
White RW, Powell R, Holland TJB et al (2014) New mineral activity-composition relations for thermodynamic calculations in metapelitic systems. J Metamorph Geol 32:261–286. https://doi.org/10.1111/jmg.12071
Yardley BWD, Bodnar RJ (2014) Fluids in the Continental Crust. Geochemical Perspect 3:1–127. https://doi.org/10.7185/geochempersp.3.1
Zen EA (1974) Prehnite- and pumpellyite-bearing mineral assemblages, west side of the appalachian metamorphic belt, pennsylvania to newfoundland. J Petrol 15:197–242. https://doi.org/10.1093/petrology/15.2.197